The initial motion of a gas bubble formed in an inviscid liquid

Part 2. The three-dimensional bubble and the toroidal bubble

By J. K. WALTERS AND J. F. DAVIDSON

Department of Chemical Engineering, Pembroke Street, Cambridge

(Received 19 November 1962 and in revised form 28 May 1963)

This paper deals with the initial motion of a gas bubble starting from rest in a liquid in the form of a sphere. Part 1 (Walters & Davidson 1962) was concerned with the similar problem of the initial motion of a two-dimensional bubble starting from rest in the form of a cylinder.

Theory and experiments like those of Part 1 are given for the present problem, and yield qualitatively similar results, the three-dimensional bubble having an initial acceleration equal to twice that of gravity, and distorting into the form of a mushroom. This distortion ultimately causes break-up, but whereas the two-dimensional bubble always detaches two small bubbles at its rear, the three-dimensional bubble breaks up into a small spherical-cap bubble with a large toroid below. A discussion of the toroidal bubble is given, and its relation to the distorted sphere from which it is formed.

The initial-motion theory is extended to deal with the problem of the growing, accelerating bubble, and leads to an expression for the volume of bubbles formed continuously at an orifice, and to a criterion for the gas flow-rate at which coalescence occurs between successive bubbles. These theoretical results are compared with experimental data from the literature and from the authors' experiments at high gas flow-rates.

1. Introduction

The analysis here presented follows the same form as for the two-dimensional case discussed in Part 1, which dealt with the initial motion of a cylindrical bubble. The essential differences are (*a*) the replacement of the trigonometrical functions by Legendre polynomials on account of the axially symmetric form of the velocity potential, and (*b*) the extension to the case of a growing bubble. This latter theory is applied to the case of continuous bubble formation at constant gas flow-rates from a submerged orifice, and gives an expression for the volume of bubbles as they detach. A criterion is also developed for the flow-rate above which double-bubble formation may be expected to occur. Ciné pictures indicate that this is substantially correct, and also show that the back of the bubble moves downwards at the start, thus justifying the assumption of Davidson & Schüler (1960) that the orifice is initially at the centre of the bubble.

The first part of the analysis also provides a way of calculating the circulation associated with a toroidal bubble. Such bubbles were produced by injecting a quantity of air into the bottom of a tank of water, and the observations show that they move with the velocity of a vortex ring whose core has the same dimensions as the bubble. The results also show that the circulation associated with the vortex ring can be calculated from the above theory of distortion of a spherical bubble.

2. The theory of the initial motion

For the case of an initially spherical bubble the velocity potential ϕ is expressed in terms of a series of Legendre polynomials P_n, thus

$$\phi = \frac{Ua^3}{2r^2}P_1 + \sum_{n=2}^{\infty}\frac{\beta_n P_n}{r^{n+1}} = \sum_{n=1}^{\infty}\frac{\beta_n P_n}{r^{n+1}}. \tag{1}$$

Here a is the initial radius of the bubble, r and θ are polar co-ordinates whose origin moves with the bubble and has an upward velocity U at time t after the start. The coefficients β_n are functions of time, and have to be adjusted so that the pressure within the bubble shall be independent of θ. The first term in (1) represents the potential due to a sphere, β_1 equalling $\frac{1}{2}Ua^3$, and the remaining terms describe the subsequent distortion of the bubble. The pressure p in the liquid is found from Bernoulli's theorem, as in Part 1,

$$\frac{p}{\rho} = \frac{\partial\phi}{\partial t} - \tfrac{1}{2}q^2 + K - g\left(\int_0^t U\,dt' + r\cos\theta\right), \tag{2}$$

where $\partial\phi/\partial t$ is the partial derivative at a fixed point in space, q is the absolute velocity and K is constant, since the pressure at infinity is presumed fixed. Following the method of Lamb (1932), as in Part 1, $\partial\phi/\partial t$ is calculated in terms of $\dot{r} = -U\cos\theta$ and $\dot{\theta} = U\sin\theta/r$, the rates of change of r and θ for a point fixed in space, so that from (1), using recursion formulae for the P_n (Magnus & Oberhettinger 1949, p. 50),

$$\frac{\partial\phi}{\partial t} = \sum_{n=1}^{\infty}\left[\frac{\dot{\beta}_n P_n}{r^{n+1}} + \frac{(n+1)\,U\beta_n P_{n+1}}{r^{n+2}}\right]. \tag{3}$$

Also, $q^2 = (\partial\phi/\partial r)^2 + (\partial\phi/\partial\theta)^2/r^2$ and again from (1), using an expression for $P_n P_m$ given by Whittaker & Watson (1927, p. 331),

$$q^2 = \frac{2\beta_1^2}{r^6}(P_0 + P_2) + 2\sum_{n=2}^{\infty}\frac{(n+1)\,\beta_1\beta_n}{(2n+1)\,r^{n+5}}[(n+2)\,P_{n+1} + 3nP_{n-1}] + O(\beta_n^2). \tag{4}$$

The pressure p_s just outside the bubble is calculated, as in Part 1, by substituting (3) and (4) into (2) with $r = R$, where R is the radius vector from the moving origin of (r, θ) to the surface of the bubble. R is then put equal to $a(1+\zeta)$, where ζ, a dimensionless function of t, θ, and a, describes the shape of the bubble. Assuming $\zeta \ll 1$ we get, from (2)–(4),

$$\frac{p_s}{\rho} = K - g\int_0^t U\,dt' - \tfrac{1}{4}U^2(1-3P_2) + \left(\frac{\dot{\beta}_1}{a^2} - ga\right)P_1 + \sum_{n=2}^{\infty}\left[\frac{\dot{\beta}_n P_n}{a^{n+1}} + \frac{3n(n+1)\,U\beta_n}{2(2n+1)\,a^{n+2}}(P_{n+1} - P_{n-1})\right] + O(\beta_n^2)_{n>1} + O(\zeta). \tag{5}$$

As in Part 1, the radius a of the bubble is assumed constant and surface tension is neglected, so that p_s is equal to the pressure within the bubble. This must be made independent of θ and equating the coefficients of P_n to zero gives the following equations for the β_n:

$$n = 1, \quad \dot{\beta}_1 - ga^3 - \tfrac{9}{5}U\beta_2/a^2 = 0, \tag{6}$$

$$n = 2, \quad \dot{\beta}_2 + \tfrac{3}{2}U\beta_1 - \tfrac{18}{7}U\beta_3/a^2 = 0, \tag{7}$$

$$n > 2, \quad \dot{\beta}_n + \frac{3n(n-1)}{2(2n-1)}U\beta_{n-1} - \frac{3(n+1)(n+2)}{2(2n+3)}\frac{U\beta_{n+1}}{a^2} = 0. \tag{8}$$

These are the equations corresponding to (6) and (7) in Part 1 for the two-dimensional bubble. In deriving (6)–(8), second-order terms in (3)–(5) were neglected; the effects of these terms, and of similar approximations below, are discussed in the Appendix to this paper. Proceeding as before by ignoring the last term in each of (6)–(8), the first approximation becomes

$$n = 1, \quad 2\beta_1^{(1)}/a^3 = U^{(1)} = 2gt, \tag{9}$$

$$n \geqslant 2, \quad \beta_n^{(1)} = \frac{(-1)^{n-1}3^n 2^{2n-3}n![(n-1)!]^3 a^3}{[(2n-1)!]^2 t}(gt^2)^n. \tag{10}$$

The shape of the bubble is calculated by equating the two expressions, $(-\partial\phi/\partial r)_{r=R}$ and $(a\dot{\zeta} + U\cos\theta)$, for the radial velocity at the bubble surface, giving

$$\dot{\zeta} + \zeta\sum_{n=1}^{\infty}\frac{(n+1)(n+2)}{a^{n+3}}\beta_n P_n = \sum_{n=2}^{\infty}\frac{(n+1)\beta_n}{a^{n+3}}P_n, \tag{11}$$

the $O(\zeta)$ terms from (1) having been retained, as in Part 1. On substituting from (9) and (10) into (11) we see that the summed terms become polynomials in $N = gt^2/a$; by equating coefficients of powers of t and using expressions for P_n given by Jahnke & Emde (1945) we obtain a series solution, the first few terms of which are

$$\zeta = -0{\cdot}750N^2P_2 + N^3(0{\cdot}93P_3 + 0{\cdot}3P_1) - N^4(1{\cdot}31P_4 + 0{\cdot}77P_2 + 0{\cdot}3). \tag{12}$$

The Appendix to this paper gives a derivation of a second approximation for ζ. This result, (37), shows that the first term in (12) is correct, the N^3 term is changed by a small amount, and the N^4 term is appreciably changed; but (12) is adequate for $N < 0{\cdot}5$, and roughly correct for somewhat larger values of N.

3. The formation of the tongue of liquid

The tongue of liquid begins to form at the back of the bubble when the curvature of the surface at that point changes sign. In polar co-ordinates, the curvature is

$$\frac{R^2 + 2(dR/d\theta)^2 - R\,d^2R/d\theta^2}{[R^2 + (dR/d\theta)^2]^{\frac{3}{2}}},$$

and hence at the back of the bubble where $\theta = \pi$ and $dR/d\theta = 0$, the curvature changes sign when $d^2R/d\theta^2 = R$. Substituting from (12) into this equation, with $R = a(1+\zeta)$ and using the first three terms, then gives $N = 0{\cdot}36$ as the point when

the tongue should begin to form. This value of N corresponds to frame 6 in figure 1, plate 1, and the tongue can be seen in the following frames as a dark patch rising from the back of the bubble.

4. Experiments with a three-dimensional bubble

It was not easy to produce a stationary spherical bubble in a stagnant liquid and several methods were tried. The most successful was to inflate a rubber balloon almost to its breaking point and then to burst it with a pin in a closed vessel completely filled with water, the rigidity of the vessel keeping the bubble at

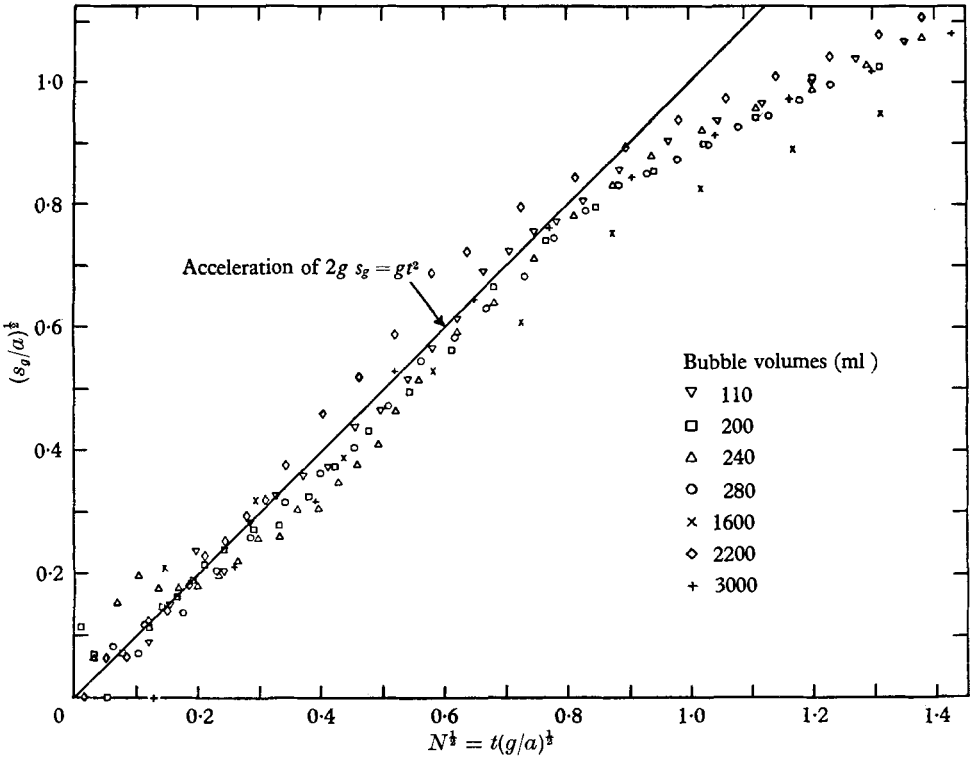

FIGURE 3. The upward displacement of a spherical bubble starting from rest.

a constant volume. The balloon was attached to a brass tube, inflated, and then clamped to a portable framework. Lead weights were used to overcome the buoyancy and hold the framework at the bottom of an 18 in. square tank about 3 ft. high made of Perspex $\frac{1}{2}$ in. thick. The lid was then screwed down and the vessel filled with water, all air being carefully expelled through a vent in the top corner. The bubble was released by bursting the balloon with a pin attached to a lever arm.

The subsequent motion of the bubble was observed photographically either with a Fastax camera at about 1000 frames/sec or with a Pathé camera at 80 frames/sec, and two typical bubbles are shown in figure 1, plate 1 and figure 2, plate 2. A millisecond time base was provided on the film for the Fastax camera while a 200 r.p.m. clock was included in the field of view for the Pathé camera

The film was analysed frame by frame by measuring the projected image of the bubble. The centroid could not be determined precisely, but since the initial distortion predicted by the first term in (12) is into an ellipsoid of revolution, it seemed reasonable to take the average position of the front and back of the bubble for comparison in figure 3. The vertical diameter was also measured, the tongue of liquid projecting upwards from the rear being visible through the bubble, and the results are presented in figure 4.

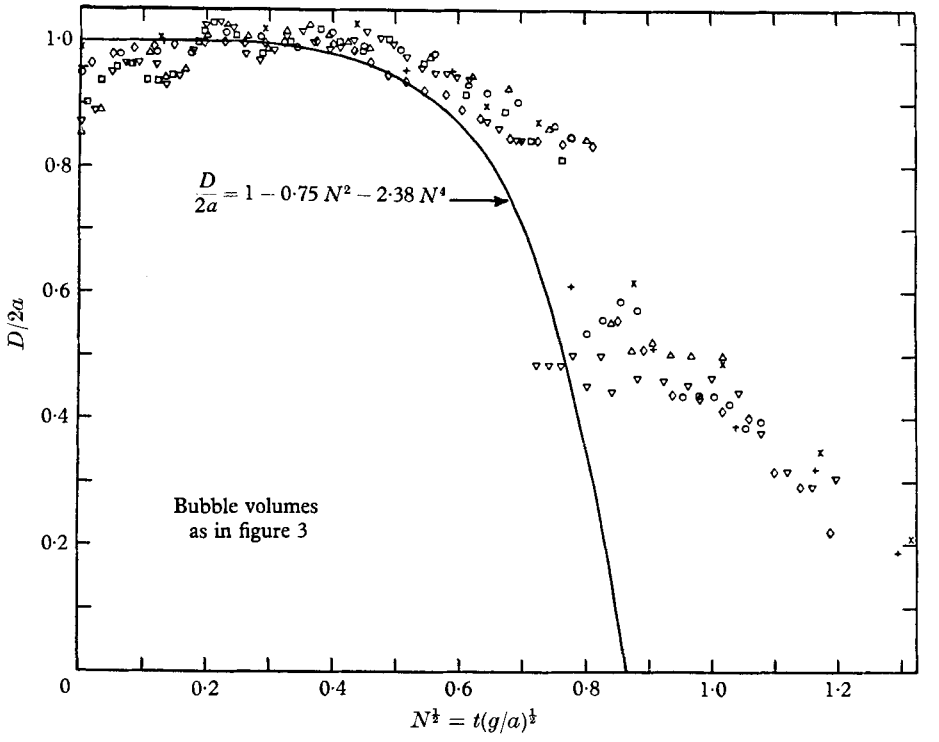

FIGURE 4. The change in vertical diameter of a spherical bubble starting from rest.

5. Comparison between theory and experiment

The balloon burst by forming a circumferential split from the point of puncture, after which the rubber peeled back along the air–water interface to leave the surface of the bubble with a crinkly appearance rather like frosted glass. This made it difficult to see the tongue of liquid that comes up from the bottom of the bubble, but it is more easily seen in the projected ciné film than in the prints in figures 1 and 2. As in the two-dimensional case, the theory, (12), predicts the formation of such a tongue of liquid, but with the change taking place rather more rapidly. Davidson & Schüler (1960) show photographs of bubbles forming at an orifice, the same type of tongue being produced just as the bubble is moving away from the orifice.

The displacement of the bubble s_g is compared with theory, (9), in figure 3. It is not obvious that the movement of the centre of co-ordinates from (9) is the same as that of the centre of gravity of the bubble; but in Part 1 it was shown, by

using the second approximation, that the two centres do in fact move together and the same is true of a three-dimensional bubble (see Appendix). The zero of time was taken as the point when the pin punctured the balloon, but the withdrawal of the rubber took about 2 or 3 msec and this is the magnitude of the difference between the theoretical line and the experimental points. There is excellent agreement up to a value of $N^{\frac{1}{2}}$ of about 0·9 showing that the bubble does in fact start to move with an acceleration of $2g$.

The photographs in figures 1 and 2 show that the balloon is approximately spherical at the start, but not precisely so. Two point support was tried but it proved unsatisfactory as the balloon did not then burst in a reproducible manner. Also, although the vessel was completely filled with water, the Perspex was sufficiently elastic to allow a slight flexing of the walls when the excess pressure was released by bursting the balloon. This caused about three initial pulsations of the bubble with period about 9 msec, but the subsequent changes of shape are in reasonable agreement with (12). The value for a was taken as the mean vertical radius during the second pulsation, because of the slight overall expansion at the start; these effects were almost negligible with the larger bubbles, but it is interesting to note that the natural period of pulsation for a 200 ml bubble in an infinite volume of water can be shown (Walters 1962) to be about 9·5 msec.

Figure 4 shows observations of the vertical height D measured on the axis of symmetry of the bubble, together with the theoretical line from (12) which is

$$D/2a = \tfrac{1}{2}(2+\zeta_0+\zeta_\pi) = 1-0{\cdot}75N^2-2{\cdot}38N^4. \tag{13}$$

This equation is likely to be seriously in error when $N > 0{\cdot}5$ owing to the approximations of the small deformation theory, discussed in detail in the Appendix. However, it is interesting to note that (13) becomes zero when $N^{\frac{1}{2}} = 0{\cdot}845$ and figures 3 and 4 indicate that a change in behaviour does occur in this region, and in the subsequent motion a small spherical-cap bubble is formed, with a toroidal bubble at the centre of a ring vortex in its wake. The circulation generated can clearly be seen on the projected ciné film, which also shows that most of the volume is contained in the toroid which, however, soon breaks up. These changes can be seen in the photographs in figure 2 and the formation of the tongue of liquid in the earlier stages is seen in figure 1, frames 7 to 11. Theoretically this tongue should begin to form when the curvature at the back of the bubble changes sign and, as shown above, this occurs at $N^{\frac{1}{2}} = 0{\cdot}6$. This point corresponds approximately to frame 6 in figure 1 and the subsequent frames in fact show the tongue, so the agreement is good. It is very difficult to locate the back of the bubble when the tongue is beginning to form and this accounts for the lack of experimental points around the ordinate value of 0·7 in figure 4.

The change from the irrotational motion in the initial stages to the fully separated flow around the spherical-cap bubble takes place in the same manner as in the two-dimensional case, and is caused by the tongue of liquid rising from the rear. Once again the vorticity associated with the separated flow is produced by the break-up of the bubble, rather than by viscous forces as in the case of the wake behind a solid object. The difference between the two- and three-dimensional bubbles is quantitative rather than qualitative; the volume of gas retained

by the spherical-cap bubble is much less in the three-dimensional case, and may be zero as described in § 10; and the detached toroid is of course a much larger proportion of the original bubble than the two detached bubbles shown in figure 2 of Part 1 in the two-dimensional case.

6. The growing three-dimensional bubble

For an expanding sphere the velocity potential is $a^2\dot{a}/r$ and so for a growing bubble we take

$$\phi = \frac{a^2\dot{a}}{r} + \frac{Ua^3}{2r^2}P_1 + \sum_{n=2}^{\infty}\frac{\beta_n P_n}{r^{n+1}} = \sum_{n=0}^{\infty}\frac{\beta_n P_n}{r^{n+1}}, \tag{14}$$

where $\beta_0 = a^2\dot{a}$, and $\beta_1 = \frac{1}{2}Ua^3$ as before. The analysis is essentially the same as that presented above in § 2 but with the addition to each equation of terms associated with β_0. Equation (3) remains of the same form but with the summation beginning at $n = 0$ rather than $n = 1$, but (4) has the additional terms

$$\frac{\beta_0^2}{r^4} + \sum_{n=1}^{\infty}\frac{2(n+1)\beta_0\beta_n}{r^{n+4}}P_n.$$

Substituting the new equations for $\partial\phi/\partial t$ and q^2 into Bernoulli's equation (2) then gives the pressure p_s at the surface of the bubble. This gives an equation like (5) but with the following terms added to the right-hand side

$$\frac{\beta_0}{a} - \frac{\dot{a}^2}{2} - \sum_{n=2}^{\infty}\frac{(n+1)\dot{a}\beta_n}{a^{n+2}}P_n.$$

The pressure p_s is again made independent of θ by equating the coefficients of P_n to zero, giving the following equations for the β_n,

$$n = 1, \quad \dot{\beta}_1 - ga^3 - \tfrac{9}{5}U\beta_2/a^2 = 0, \tag{15}$$

$$n = 2, \quad \dot{\beta}_2 - 3\dot{a}\beta_2/a + \tfrac{3}{2}U\beta_1 - \tfrac{18}{7}U\beta_3/a^2 = 0, \tag{16}$$

$$n > 2, \quad \dot{\beta}_n - (n+1)\frac{\dot{a}\beta_n}{a} + \frac{3n(n-1)\,U\beta_{n-1}}{2(2n-1)} - \frac{3(n+1)\,(n+2)\,U\beta_{n+1}}{2(2n+3)\,a^2} = 0. \tag{17}$$

Because the bubble is expanding, its radius a is not constant and will be given by

$$Gt = 4\pi a^3/3, \quad \text{so that} \quad G = 4\pi a^2\dot{a}, \tag{18}$$

where G is the volumetric flow rate of gas into the bubble. The simplest case to consider is when G is constant, and substituting from (18) into (15)–(17), and integrating, gives for the first approximation

$$n = 1, \quad 2\beta_1^{(1)}/a^3 = U^{(1)} = gt, \tag{19}$$

$$n \geqslant 2, \quad \beta_n^{(1)} = \frac{(-1)^{n-1}\,3^{2n}(n-1)!\,(n!)^2\,G}{8\pi(2n)!\,9.14\ldots(5n-1)}(gt^2)^n. \tag{20}$$

These are obtained by omitting the last term in each of (15), (16) and (17) and using repeated integration n times with the integrating factor $t^{-\frac{1}{3}(n+1)}$ each time.

The shape of the bubble is calculated in the same way as before by equating the two expressions, $-\partial\phi/\partial r$ and $a\dot{\zeta}+\dot{a}(1+\zeta)+U\cos\theta$, for the radial velocity at the bubble surface, giving

$$\dot{\zeta}+\zeta\left[\frac{3\dot{a}}{a}+\sum_{n=1}^{\infty}\frac{(n+1)(n+2)}{a^{n+3}}\beta_n P_n\right]=\sum_{n=2}^{\infty}\frac{(n+1)}{a^{n+3}}\beta_n P_n. \tag{21}$$

Substituting from (19) and (20) and solving as before gives

$$\begin{aligned}\zeta = &-0{\cdot}173N^2P_2+N^3(0{\cdot}116P_3+0{\cdot}346P_1)\\ &-N^4(0{\cdot}0863P_4+0{\cdot}0477P_2+0{\cdot}0181).\end{aligned} \tag{22}$$

It is probable that the N^4 term is inaccurate because of error terms like those discussed in the Appendix. Comparing (22) and (12) the general behaviour is seen to be the same as for the non-expanding bubble, but the expansion term causes the changes of shape to occur much more slowly. It is also interesting that (19) indicates an upward acceleration of g in contrast to that of $2g$ for the non-expanding bubble. This difference is explained by the simple theory of Davidson & Schüler (1960) who assumed that the forming bubble is always spherical. On this basis the rate of change of upward momentum is $d(\frac{1}{2}\rho VU)/dt$, V being the volume and ρ the liquid density. The bubble can therefore acquire momentum on account of growth as well as on account of acceleration, so the latter must be smaller for a growing bubble.

Since G has been assumed fixed, the above theory is applicable to the case of continuous bubble formation from an orifice to which the gas is supplied at a constant volumetric flow-rate. Following the model put forward by Davidson & Schüler (1960) we imagine the gas to be supplied from a fixed-point source within the liquid, so that ideally the bubble will detach itself when it has risen a distance such that its back is level with the source, when

$$\int_0^t U\,dt' = a(1+\zeta_\pi).$$

Here ζ_π is the shape factor at the back of the bubble where $\theta=\pi$. Substituting from (19) and (22) gives an equation for N, the solution of which is $N=1{\cdot}013$. Combining this with the first of (18) then gives for the bubble volume

$$V = 0{\cdot}76g^{-\frac{3}{5}}G^{\frac{6}{5}}. \tag{23}$$

This equation is of the same form as Davidson & Schüler's (1960) result but with a different numerical constant. Using their theory but with the effective inertia of the bubble equal to $\frac{1}{2}\rho V$, it is easily shown that the constant is 1·138. It is quite certain that the multiplying constant in (13) should be less than 1·138, because the distortion of the bubble makes it detach earlier from the orifice than if it had remained spherical. But the value of 0·76 is in error because

(*a*) the use of a finite number of terms in (22) leads to an overestimate of N at bubble detachment, and

(*b*) the use of the first approximation in the derivation of (22) leads to errors like those discussed in the Appendix, but less serious for the following reason: in the present case we are dealing with the detachment of a bubble from an

orifice, and at the instant of detachment the radial distortion is of the same order as the bubble radius; in the constant volume case discussed in the Appendix we are interested in the point of bubble break-up, when the radial distortion is of the same order as the bubble diameter.

The effect of these errors is hard to estimate, but (23) is probably correct to 10 %.

7. Multiple bubble formation

Coalescence of bubbles forming at an orifice has been reported frequently in the literature at the larger flow rates, and by an extension of the above theory it is possible to estimate the flow-rate G at which this may be expected to occur. We shall take as the criterion for this multiple bubble formation the condition when the velocity v_π of the rear surface of the bubble that has just left the orifice is equal to the velocity v_0 of the front of the next bubble.

The velocity v_π can be calculated from the above theory, but difficulty arises because of divergence of the series for $\dot{\zeta}$ near $N = 1$. Because of this difficulty, the theory of Davidson & Schüler is used to calculate the upward velocity of the bubble at detachment, which is $U = 1{\cdot}138 g^{\frac{2}{5}} G^{\frac{1}{5}}$, using an effective inertia of $\frac{1}{2}\rho V$.

To find the velocity v_0 of the front of the next bubble we assume that the preceding bubble leaves a small nucleus of air at the orifice, the radius of which is equal to that of the orifice, a_0, so that

$$v_0 = G/4\pi a_0^2,$$

then the condition $v_0 \geqslant U$ for coalescence to occur gives as the criterion for multiple bubble formation

$$G \geqslant 28 g^{\frac{1}{2}} a_0^{\frac{5}{2}}. \tag{24}$$

8. Experiments on continuous bubble formation

All previous workers have confined their attention to bubble formation at small gas flow-rates, so the present work was performed in the range 600 ml/sec to 10 l/sec. Air from the main was metered through a rotameter and then led through a $\frac{1}{2}$ in. diameter copper tube to the bottom of an open Perspex tank 18 in. square and 3 ft. high which was filled with water. Three different orifices were used, $\frac{1}{2}$ in., $\frac{3}{4}$ in. and 1 in. in diameter and the bubble formation was observed photographically with the Pathé camera set at 80 frames/sec, a clock rotating at 200 r.p.m. also being included in the field of view to give an accurate time scale. The bubble volumes were determined by two methods, first, from the frequency obtained by counting bubbles, and secondly from the mean dimensions of several bubbles measured from the projected film. In the latter case the horizontal and vertical diameters of each bubble were measured and the volume found by assuming the bubble to be an ellipsoid of revolution about the vertical axis. The photographs in figure 6, plate 3, show considerable variation in bubble shape, but the two methods are in good agreement, and the results are shown in figure 5.

9. Discussion

Equation (23) for the bubble volume is of the same form as Davidson & Schüler (1960) obtained by equating the buoyancy force to the rate of change of upward momentum, assuming the bubble remained spherical throughout its formation. They took the value $11\rho V/16$ for the virtual mass of the bubble and obtained 1·378 as the coefficient in (23). This value of the virtual mass is appropriate to a sphere moving perpendicularly near to a wall, and so the result is more

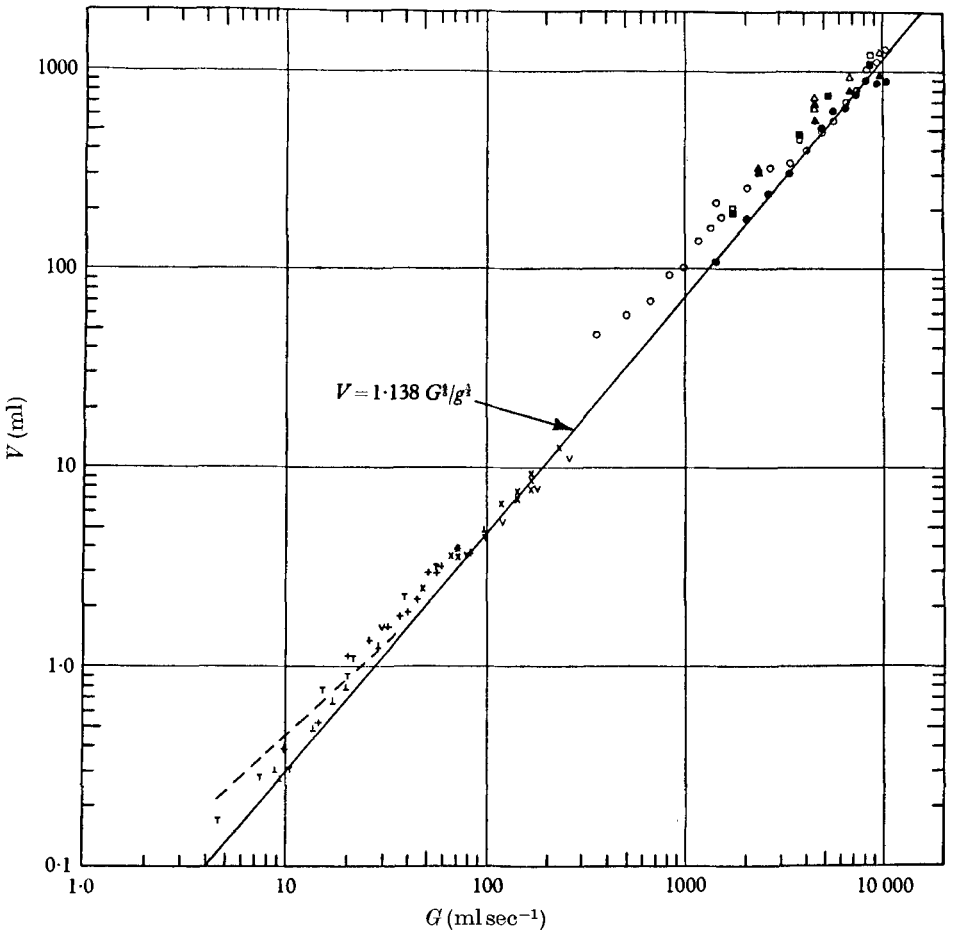

FIGURE 5. Bubble volume as a function of gas flow-rate. Present work, air–water: ○ ●, ½ in. diameter tube; □ ■, ¾ in. diameter tube; △ ▲, 1 in. diameter tube; bubble volume from counting for open points, measurement for solid points. Calderbank (1956) air–water: +, 0·265 cm capillary, ×, slots $\frac{1}{16}$ to $\frac{1}{4}$ in. wide. Van Krevelen & Hoftijzer (1950): T, 0·23 cm capillary, air–water; ⊥, H_2–water. Davidson & Amick (1956): V, 0·48 cm diameter orifice, air–water. Davidson & Schüler (1960): ---, 0·15 to 0·25 cm diameter orifices, air–water.

applicable to bubbling from a hole in a plate. The virtual mass associated with a sphere in an unbounded liquid is $\frac{1}{2}\rho V$ and this gives a coefficient of 1·138. Figure 5 shows that (23) with this coefficient gives an excellent fit over the whole range of gas flow-rates, and it is of interest to note that van Krevelen & Hoftijzer

(1950) also obtained this form of equation although their theoretical approach was somewhat different. They obtained a coefficient of 1·72. It would thus seem that the changes of shape predicted by the present theory are inhibited to such an extent by the presence of the orifice that Davidson & Schüler's assumption, that the bubble remains spherical, is well justified. The tongue of liquid at the back of the bubble does appear, however, after the bubble has left the orifice. It can be clearly seen in the photographs of Davidson & Schüler, and good pictures are also given by Helsby & Tuson (1955).

The criterion (24) for multiple bubble formation gives values of the gas flow for the three orifices used of 282, 776 and 1600 ml/sec, respectively, and figure 6, plate 3, shows ciné photographs of bubbles forming at the 1 in. orifice for four flow-rates above the critical value. These indicate that there is a gradual transition rather than any sharp change in behaviour; at low flows coalescence occurs some distance above the orifice and as the flow is increased, the coalescence point moves downwards. Good descriptions of coalescence are given by Helsby & Tuson (1955) and also by Davidson & Amick (1956). These latter authors give 30–40 ml/sec as the flow-rate for coalescence at an orifice of radius 0·16 cm, and (24) gives 9 ml/sec as the critical value. Davidson & Schüler's photographs with $G = 13{\cdot}7$ ml/sec and $a_0 = 0{\cdot}2$ cm show coalescence occurring about two or three bubble diameters above the orifice and (24) gives $G = 16$ ml/sec for coalescence at the orifice itself. Thus although there is no sharp change, (24) does give the right order of magnitude for the transition over a wide range of gas flow-rates. While it is not claimed to be a rigorous result, it may well be useful as a design criterion for the upper limit of steady bubbling from a given orifice.

10. The toroidal bubble

During the preliminary experiments designed to produce the spherical bubble described in §4, ring-shaped or toroidal bubbles were sometimes observed. However, a more reproducible method of forming toroidal bubbles was found to be the injection of a single pulse of air through a small tube inserted into the bottom of a large Perspex tank filled with water. The air was previously contained in a small vessel and let into the tank by quickly opening and closing a valve, different injection times and vessel pressures producing different bubble volumes. On leaving the orifice the bubble was moving with a large velocity, but after it had travelled a short distance the front surface slowed down, and was penetrated by the tongue of liquid from the back, thus forming a toroidal bubble. The plane of the ring was perpendicular to the direction of motion, and as the bubble moved steadily upwards its velocity decreased and the ring diameter increased. Ciné photographs of each bubble were taken with the Pathé camera at about 80 frames/sec, and figure 7, plate 4, shows three pictures taken at about $\frac{1}{4}$ sec intervals. The lower half of each frame shows the elevation through the side of the tank, whilst the top portions show the plan view obtained by reflexion in a mirror supported at 45° above the tank. In the third picture the bubble is about to break the surface, which is clearly seen erupting some distance ahead of the bubble. The filmed record of each toroidal bubble was analysed frame by frame,

enabling the ring dimensions and displacement *vs* time curves to be obtained for each bubble. The gradient of these curves then gave the bubble velocity at each instant, and the bubble volume was calculated from the ring dimensions.

Taking the bubble to be the core of a ring vortex, the velocity u is given by Lamb (1932, p. 241) as

$$u = \frac{\Gamma}{2\pi d}\left(\ln\frac{8d}{h} - \frac{1}{4}\right), \tag{25}$$

where d is the ring diameter, h the core diameter, and Γ the associated circulation. Figure 8 shows $ud/[\ln(8d/h) - \frac{1}{4}]$ plotted *vs* time for three bubbles and indicates

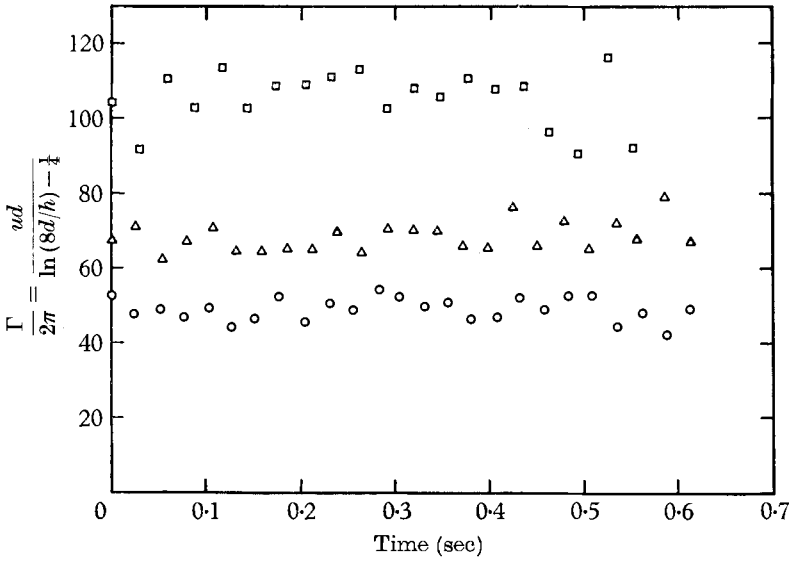

FIGURE 8. Circulation *vs* time for three toroidal bubbles.
Bubble volumes: ○, 21 ml; △, 43 ml; □, 88 ml.

that Γ remains substantially constant as the bubble rises. Thus it is the injection of the bubble and its subsequent changes of shape that cause the growth of the circulation. Once the toroid has been formed the results in figure 8 show that there is no further increase in Γ. We may obtain an estimate of the order of magnitude of this circulation by assuming that the bubble is initially spherical and that it moves according to the analysis in § 2. Referring to figure 9, $\int q.ds$ from A to E is calculated by integrating round the path ABCDE. We then assume that the bubble turns into a toroid by the liquid at E making contact with the liquid at A, and that $\int q.ds$, defined above, is equal to Γ the circulation associated with the resulting toroid. Hence

$$\Gamma = \phi_A - \phi_E,$$

where ϕ_E is the velocity potential at the rear of the bubble ($\theta = \pi$) and ϕ_A that at the front ($\theta = 0$). Substituting from (1) putting $r = a(1+\zeta)$ then gives

$$\Gamma = \sum_{n=1,3,5\ldots}^{\infty} \frac{2\beta_n}{a^{n+1}} - \sum_{n=1,2,3\ldots}^{\infty} \frac{(n+1)\beta_n}{a^{n+1}}[\zeta_0 - \zeta_\pi(-1)^n],$$

and further substitutions from (9), (10) and (12) give, keeping terms up to N^4,

$$\Gamma = 0{\cdot}98(gVN)^{\frac{1}{2}}(1+2{\cdot}2N^2+5{\cdot}8N^4). \tag{26}$$

The value of Γ associated with the toroidal bubble is given by inserting the value of N at which the toroid is formed, when the tongue of liquid from the base of the

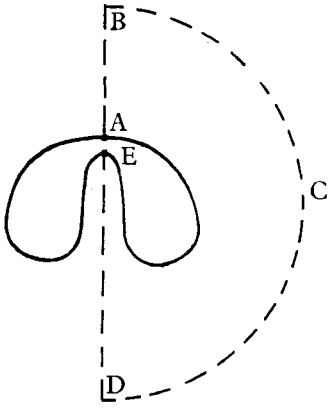

FIGURE 9. Accelerating bubble on the point of forming into a toroidal bubble.

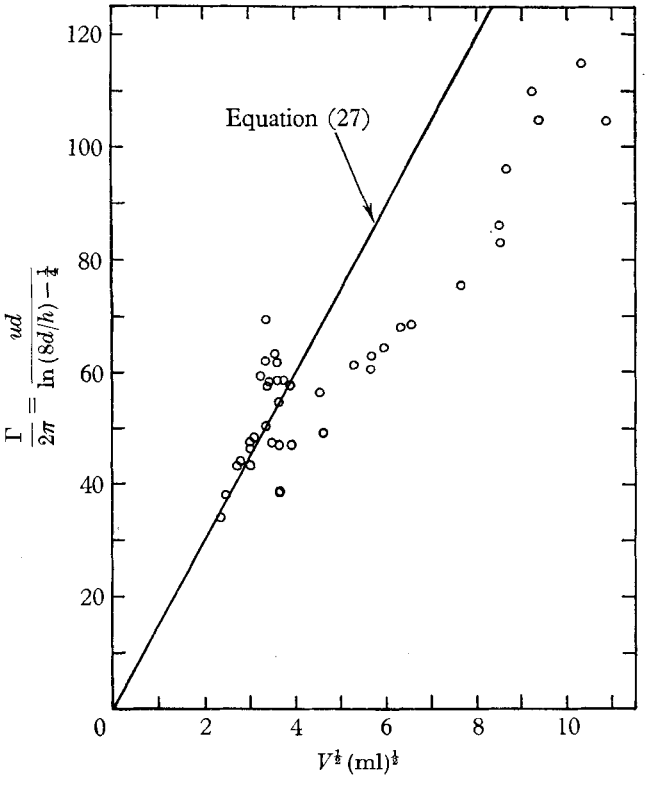

FIGURE 10. Circulation *vs* (volume)$^{\frac{1}{3}}$ for toroidal bubbles.

bubble makes contact with the top. Although at this stage the deviations of the bubble shape from sphericity are clearly not small, and the approximations of § 2 are therefore invalid, it is worth while to use the small deformation theory to get an order of magnitude for Γ. Accordingly we solve (13) with $D = 0$, giving $N = 0{\cdot}715$ and substitute this value into (26), giving

$$\Gamma = 3g^{\frac{1}{2}}V^{\frac{1}{2}}. \tag{27}$$

This is clearly only a rough approximation, since the behaviour of the three terms in (26) suggests that they are part of a divergent series, and this is in accordance with the fact that the deviations from sphericity are large. Nevertheless, (27) is in reasonable agreement with the experimental data shown in figure 10. Each point on figure 10 was derived from a plot like those in figure 8, the value of Γ for each bubble thus being a mean value derived from a number of measurements of u, d, and h.

J. K. W. wishes to acknowledge the financial assistance of a Research Studentship from the Department of Scientific and Industrial Research throughout the duration of this work.

Appendix

In Part 1 there was a discussion of the magnitude of terms neglected in deriving the first approximation $\beta_n^{(1)}$, and a second approximation $\beta_n^{(2)}$ was derived. However, further consideration shows that only the first of these, $\beta_1^{(2)}$, is truly a second approximation, and the higher terms, $\beta_2^{(2)}$, $\beta_3^{(2)}$, etc., given by (9) in Part 1, are little more accurate than the first approximation. The discussion below gives, for the spherical bubble, a more detailed analysis of the error terms, and a second approximation correct as far as $\beta_3^{(2)}$ is derived. This shows that the first approximation is valid for $N \ll 1$, but seriously in error when $N \to 1$; of course all the infinite series involved in the solution diverge in the region of $N = 1$, so that for practical purposes the second approximation is not of much more use than the first. But the second approximation does give some idea of the maximum value of N for which the first approximation is reasonably accurate, and this maximum value is probably not much more than 0·5.

Second approximation, for the non-expanding bubble

In Part 2, § 2, which gives the theory of distortion of a bubble of constant volume, terms in (4) and (5) were neglected in order to derive approximate results, (9), (10) and (12), giving the distortion of the bubble as a function of time. These approximate results will now be used to estimate the order of magnitude of the neglected terms, which are then used to derive the second approximation.

In (4), the first of the $O(\beta_n^2)$ terms, giving the error in $\frac{1}{2}q^2$ is

$$\Delta_1(\tfrac{1}{2}q^2) = (\beta_2^2/a^8)\,(1{\cdot}5 + 1{\cdot}71P_2 + 1{\cdot}29P_4), \tag{28}$$

putting $R \simeq a$ at the surface of the bubble.

In (5) there are errors derived from (28), and from putting $R = a$ instead of $R = a(1+\zeta)$ as it should. The latter approximation leads to the following errors in (5), derived from (2),

$$\Delta\left(\frac{\partial\phi}{\partial t}\right) = \sum_{n=1}^{\infty}\left[\frac{-(n+1)\dot{\beta}_n P_n \zeta}{a^{n+1}} - \frac{(n+1)(n+2)U\beta_n P_{n+1}\zeta}{a^{n+2}}\right], \tag{29}$$

$$\Delta_2(\tfrac{1}{2}q^2) = \frac{-\beta_1^2(P_0+P_2)\,6\zeta}{a^6} - \sum_{n=2}^{\infty}\frac{(n+1)\beta_1\beta_n}{(2n+1)a^{n+5}}[(n+2)P_{n+1}+3nP_{n-1}](n+5)\zeta, \tag{30}$$

$$\Delta(gr\cos\theta) = ga\zeta P_1. \tag{31}$$

In deriving (29) and (30), terms like $1/R^n$ were replaced by $(1/a^n)(1-n\zeta)$ so that the error terms (29) and (30) represent the first of a series of terms involving ζ^2, ζ^3, etc.

Using the first terms of the series in (29) and (30) we get

$$\Delta\left(\frac{\partial\phi}{\partial t}\right) \simeq \frac{-2\dot{\beta}_1}{a^2}P_1\zeta - \left(\frac{3\dot{\beta}_2+6U\beta_1}{a^3}\right)P_2\zeta, \tag{32}$$

$$\Delta_2(\tfrac{1}{2}q^2) \simeq \frac{-6\beta_1^2(P_0+P_2)\zeta}{a^6} - \frac{42\beta_1\beta_2}{5a^7}(2P_3+3P_1)\zeta. \tag{33}$$

Approximate expressions for these errors are now obtained by substituting for β_1, β_2 and ζ from (9), (10), and (12), giving, after simplification, from (28), (31), (32) and (33),

$$\begin{aligned}&\Delta(\partial\phi/\partial t) - \Delta_1(\tfrac{1}{2}q^2) - \Delta_2(\tfrac{1}{2}q^2) - \Delta(gr\cos\theta)\\ &\quad = (a^2/t^2)(-2{\cdot}25N^4 + 0{\cdot}9N^3P_1 - 8{\cdot}65N^4P_2 + 1{\cdot}35N^3P_3 - 4{\cdot}04N^4P_4).\end{aligned} \tag{34}$$

The next step is to equate to zero the coefficients of P_n in (5), so as to make the pressure within the bubble independent of θ, and including the terms from (34), and the last terms in each of (6)–(8), we get

$$\left.\begin{aligned}\dot{\beta}_1^{(2)} - ga^3 - 9U^{(1)}\beta_2^{(1)}/5a^2 + 0{\cdot}9N^3a^4/t^2 &= 0, \quad \text{(i)}\\ \dot{\beta}_2^{(2)} + \tfrac{3}{2}U^{(2)}\beta_1^{(2)} - \tfrac{18}{7}U^{(1)}\beta_3^{(1)} - 8{\cdot}65N^4a^5/t^2 &= 0, \quad \text{(ii)}\\ \dot{\beta}_3^{(2)} + \tfrac{9}{5}U^{(1)}\beta_2^{(1)} + 1{\cdot}35N^3a^6/t^2 &= 0, \quad \text{(iii)}\\ \dot{\beta}_4^{(2)} + \tfrac{18}{7}U^{(1)}\beta_3^{(2)} - 4{\cdot}04N^4a^7/t^2 &= 0. \quad \text{(iv)}\end{aligned}\right\} \tag{35}$$

In (35 iii), it was sufficiently accurate to omit the term $U\beta_4$ and to use $U^{(1)}\beta_2^{(1)}$ instead of $U^{(2)}\beta_2^{(2)}$. Similarly in (35 iv) it was possible to omit the term $U\beta_5$ though it was necessary to use $U^{(1)}\beta_3^{(2)}$ rather than $U^{(1)}\beta_3^{(1)}$, because β_3 changes more than β_2 in the second approximation.

Integrating (35) gives the following expressions for $\beta_1^{(2)}$, etc.,

$$\left.\begin{aligned}\beta_1^{(2)} &= Na^4(1-0{\cdot}9N^2)/t, \quad & \beta_2^{(2)} &= -N^2a^5(1-2{\cdot}54N^2)/t,\\ \beta_3^{(2)} &= 0{\cdot}45N^3a^6/t, & \beta_4^{(2)} &= 0{\cdot}246N^4a^7/t.\end{aligned}\right\} \tag{36}$$

Using the above expressions for $\beta_1^{(2)}$, etc., in (11) gives a second approximation for ζ,

$$\zeta = -0{\cdot}75N^2P_2 + N^3(0{\cdot}75P_3 + 0{\cdot}3P_1) - N^4(0{\cdot}746P_4 - 0{\cdot}24P_2 + 0{\cdot}3). \tag{37}$$

Comparison with (12) shows that there is a small change in the N^3 term, and there are considerable changes in the N^4 term. Examination of the derivation shows that a third approximation would change only the N^4 term in (37), but not the N^2 and N^3 terms. From (37) it is easy to get an expression for the central height D of the bubble,

$$D/2a = 1 - 0{\cdot}75N^2 - 0{\cdot}806N^4. \tag{38}$$

Although the third term of (38) is very different from the corresponding term in (13), the difference in the estimated value of D is small for $N < 0{\cdot}5$; of course the value of N to give $D = 0$ is considerably different ($N = 0{\cdot}715$ from (13) and $0{\cdot}861$ from (38)), but for these values of N the whole method of solution breaks down, because the deformation of the bubble is of the same order as its radius.

Motion of the centroid

If s is the distance moved by the centre of co-ordinates, and s_g the distance moved by the centroid,

$$s_g - s = \frac{3a}{2}\int_0^\pi \zeta \sin\theta \cos\theta \, d\theta$$

(cf. (15) in Part 1 of this paper), and substituting from (37) gives $s_g - s = 0{\cdot}3N^3a$. By integrating the first of (36), we get $s = Na(1 - 0{\cdot}3N^2)$, so that $s_g = Na$; this means that the centroid has an acceleration of exactly $2g$.

REFERENCES

CALDERBANK, P. H. 1956 *Trans. Inst. Chem. Engrs*, **34**, 79.

DAVIDSON, L. & AMICK, E. H. 1956 *A.I.Ch.E. J.* **2**, 337.

DAVIDSON, J. F. & SCHÜLER, B. O. G. 1960 *Trans. Inst. Chem. Engrs*, **38**, 335.

HELSBY, F. W. & TUSON, K. R. 1955 *Research*, **8**, 270.

JAHNKE, E. & EMDE, F. 1945 *Tables of Functions*, 4th ed., p. 108. New York: Dover.

LAMB, SIR HORACE 1932 *Hydrodynamics*, pp. 239, 241. Cambridge University Press.

MAGNUS, W. & OBERHETTINGER, F. 1949 *Special Functions of Mathematical Physics*, p. 50. New York: Chelsea Publishing Co.

VAN KREVELEN, D. W. & HOFTIJZER, P. J. 1950 *Chem. Engng Progr.* **46**, 29.

WALTERS, J. K. 1962 Bubble motion and leakage from sieve trays. Ph.D. dissertation, University of Cambridge.

WALTERS, J. K. & DAVIDSON, J. F. 1962 *J. Fluid Mech.* **12**, 408.

WHITTAKER, E. T. & WATSON, G. N. 1927 *Modern Analysis*, 4th ed., p. 331. Cambridge University Press.

Errata to Part 1

The third term in equation (13) should read

$$-0{\cdot}0612N^4(\cos 4\theta + \ldots$$

and the second reference should read

DAVIES, R. M. & TAYLOR, SIR GEOFFREY 1950 *Proc. Roy. Soc.* A, **200**, 375.

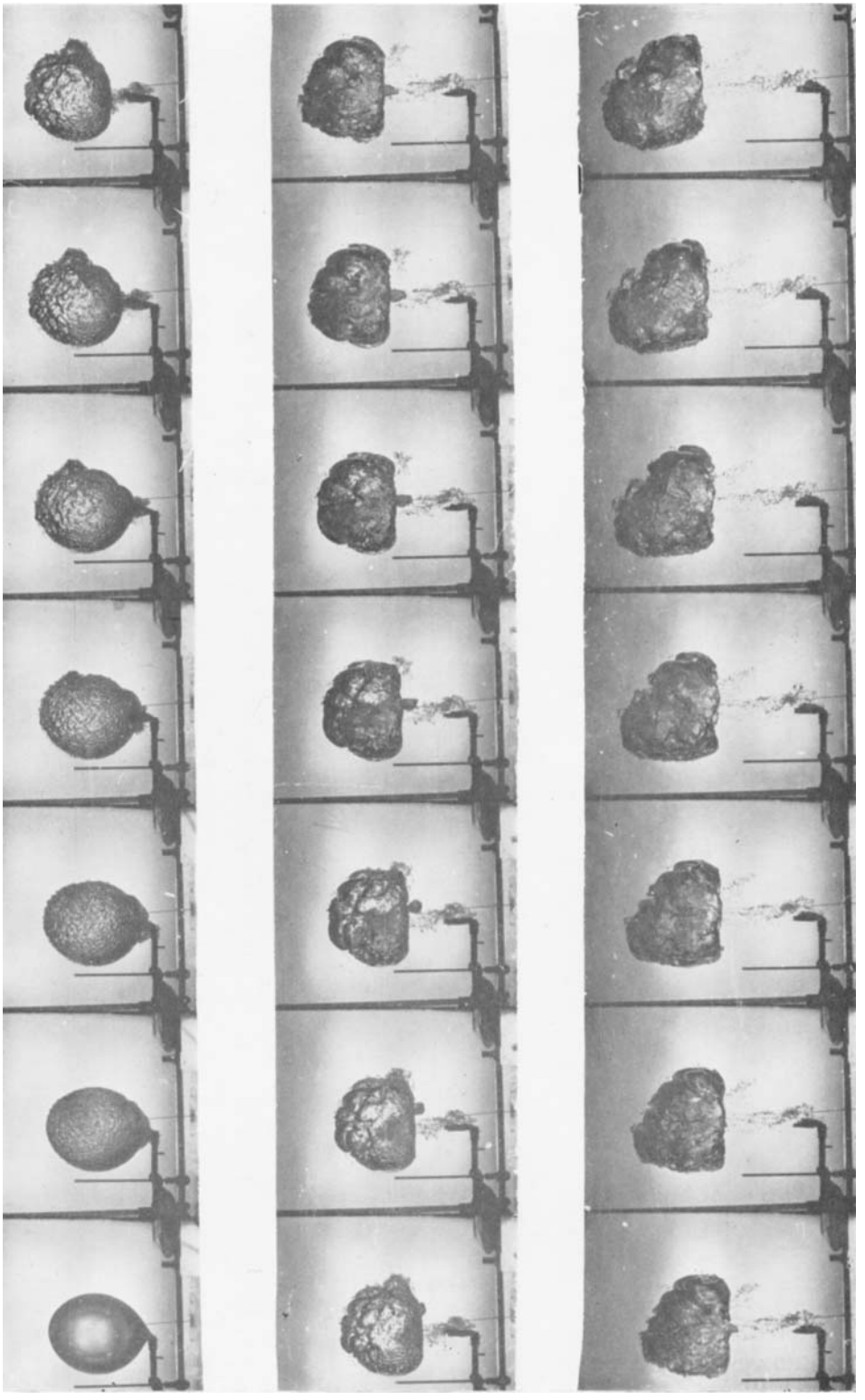

FIGURE 1. Ciné pictures at about 80 frames/sec of the initial motion of a 3000 ml bubble.

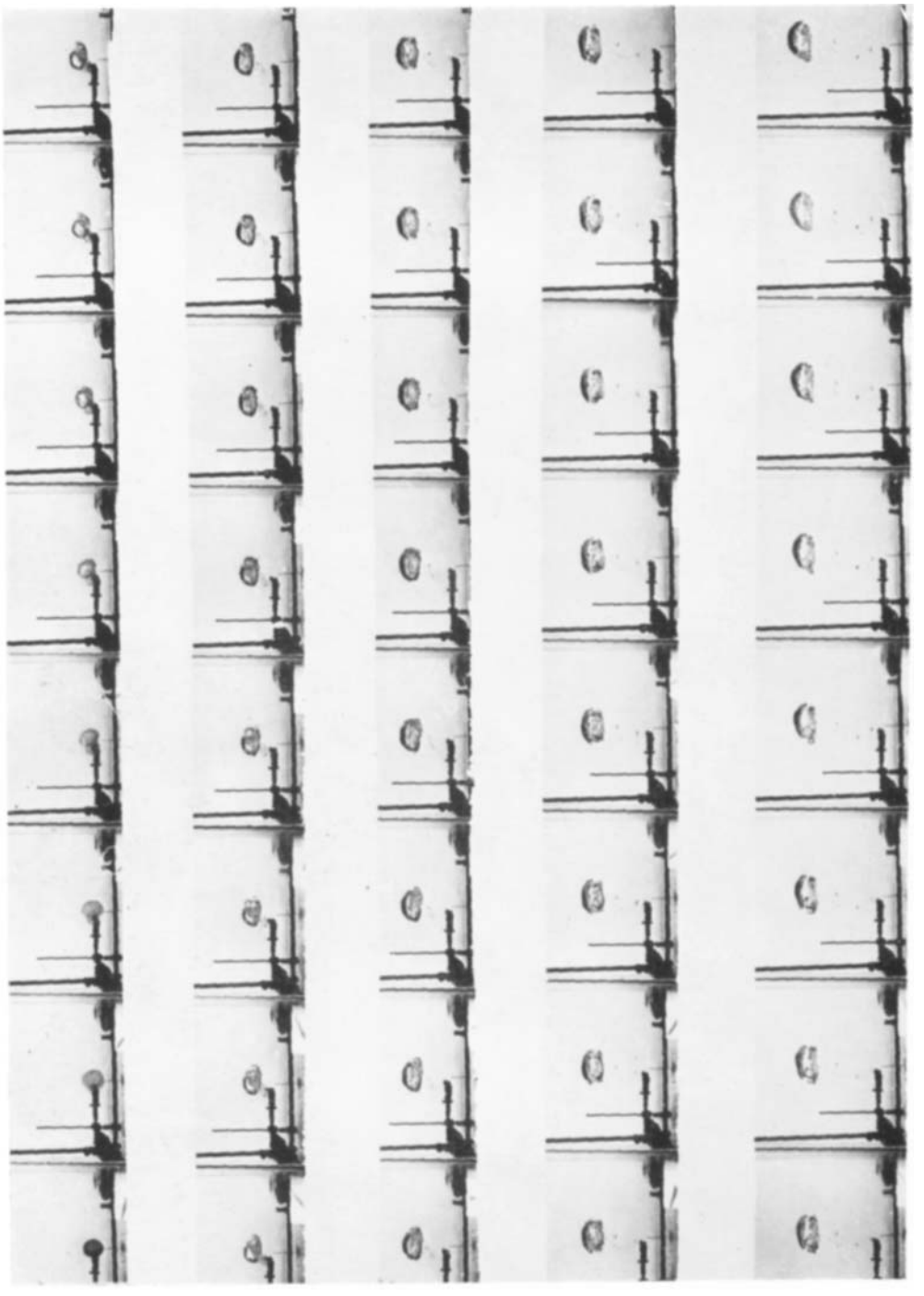

FIGURE 2. Ciné pictures at about 80 frames/sec of the initial motion of a 100 ml bubble.

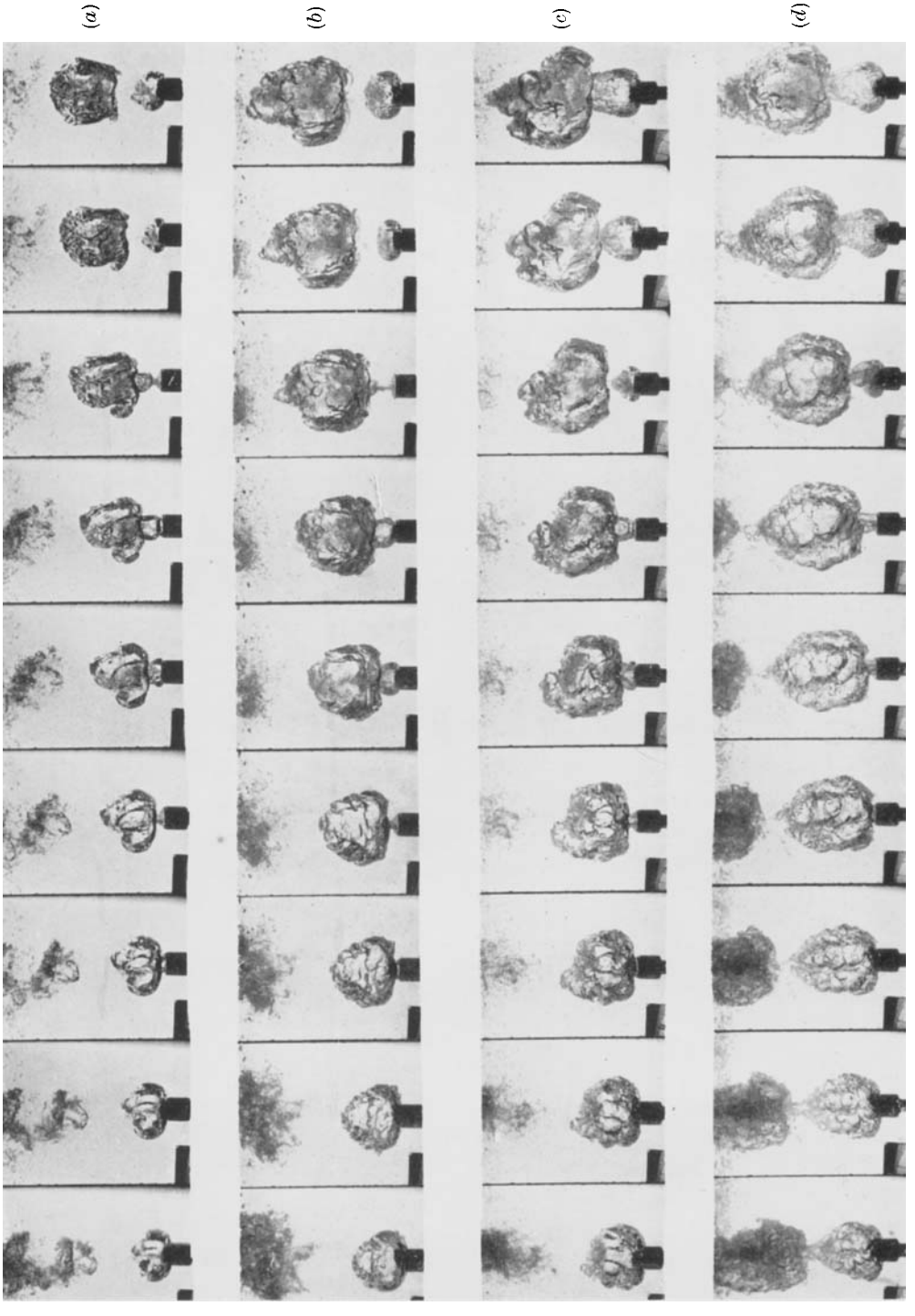

FIGURE 6. Ciné pictures at about 80 frames/sec of bubbles forming from a 1 in. diameter tube. Flow rates: (*a*), 2·34; (*b*), 4·49; (*c*), 6·75; (*d*), 9·65 l/sec respectively.

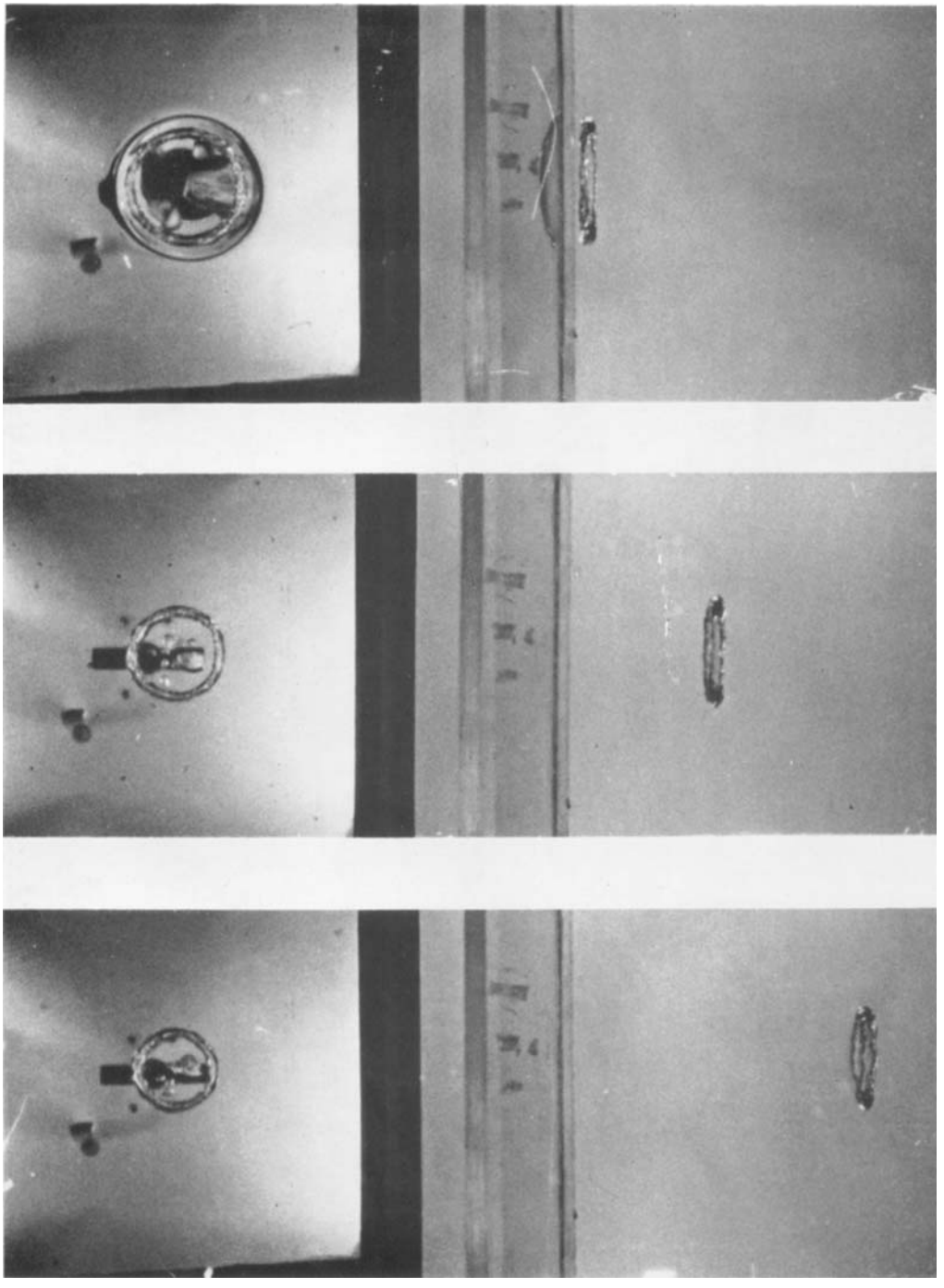

FIGURE 7. A toroidal bubble at intervals of about $\frac{1}{4}$ sec. Ring diameter approximately 8 cm.